TECHNICAL MEMORANDUMS

NATIONAL ADVISORY COMMITTEE FOR AERONAUTICS

No. 848

PLANING-SURFACE TESTS AT LARGE FROUDE

NUMBERS - AIRFOIL COMPARISON

By A. Sambraus

Washington
February 1938

NATIONAL ADVISORY COMMITTEE FOR AERONAUTICS

TECHNICAL MEMORANDUM NO. 848

PLANING-SURFACE TESTS AT LARGE FROUDE

NUMBERS - AIRFOIL COMPARISON*

By A. Sambraus

INTRODUCTION

The take-off capacity of a flying boat depends upon the design of the hull bottom ahead as well as aft of the step. Systematic tests - largely made by the industry itself - had proved the benefit accruing from a well-designed hull bottom long before theoretical insight into the flow phenomena involved had been obtained. The theoretical framing of the problem was beset with serious difficulties and, though restricted to the processes within range of the planing bottom ahead of the step, the solutions do not as yet afford a comprehensive survey.

NOTATION

Planing
surface,
airfoil

g,   acceleration of gravity.

$\rho = \gamma/g$,   density.

V   plate speed.

$V_1 = V\beta$,   vertical speed component at planing surface.

b,   plate width (at right angles to V).

l,   plate length (in V direction) (for planing
            surface = area of pressure surface divided
            by b).

Planing surface	Airfoil	
	l_p	distance of lift resultant from trailing edge of plate.
$t = l\,\beta$		depth of immersion.
β		angle of attack of plate.
	β_w	"effective" angle of attack = β minus angle of downwash β_1.
$\Delta\beta_w$		supplementary angle of attack due to boundary-layer friction at planing surface.
$\beta_1 = \dfrac{4R}{\pi\rho V^2 b^2}$	$\beta_1' = \dfrac{2R'}{\pi\rho V^2 b^2}$	angle of downwash due to infinite width of surface in motion free from gravity.
	$F = \dfrac{V}{\sqrt{bg}}$	Froude number.
	$R = \dfrac{V\,l}{\nu}$	Reynolds Number.
$\dfrac{R}{\frac{\rho}{2}V^2 b^2}$		load factor.
	G_V	forward plate loading.
	G_H	rear plate loading.
B	B'	momentum of downward moving fluid mass.
$m_0 = \dfrac{\rho}{2}\dfrac{\pi b^2}{4}$	$m_0' = \rho\,\dfrac{\pi b^2}{4}$	mass reduced to V_1 moving downward per length "one" at infinitely small angle of attack.
m	m'	mass reduced to V_1 moving downward per length "one" at finite angle of attack.

Planing surface	Airfoil	
R_0	R_0'	normal force of plate at infinitely small angle of attack.
R	R'	normal force of plate at finite angle of attack (fig. 1).
$A_0 = R_0 \cos \beta$	$A_0' = R_0' \cos \beta$	lift at infinitely small angle of attack.
$A = R \cos \beta$	$A' = R' \cos \beta$	lift at finite angle of attack.
$\mu = \dfrac{m}{m_0} = \dfrac{A}{A_0}$	$\mu' = \dfrac{m'}{m_0'} = \dfrac{A'}{A_0'}$	conversion factor.
$c_a = \dfrac{A}{\dfrac{\rho}{2} V^2 b\, l}$	$c_a' = \dfrac{A'}{\dfrac{\rho}{2} V^2 b\, l}$	lift coefficient.
W_Z		horizontal push-rod force.
W_R		frictional drag in boundary-layer drag coefficient.
$c_f = \dfrac{W_R}{\dfrac{\rho}{2} V^2 b\, l}$		drag coefficient.
κ		auxiliary quantity (taken from fig. 18 of reference 2).

PART I

1. Previous Studies

In his method of explaining the case of accelerated planing, H. Wagner (references 1 and 2) disregarded both the gravity and the fluid viscosity. He observed that, in accelerated planing at very (infinitely) small angles of attack, the lift of a planing surface is exactly half as great as that of an identical infinitely thin airfoil whose plan corresponds to the wetted surface (pressure surface) (airfoil comparison).

The attempt at reconciling Wagner's theory (references 1 and 2) with Sottorf's test data on flat planing surfaces (references 3, 4, and 5) was quite satisfactory (curve C, figs. 14 and 16) for short plates (i.e., for small l/b) up to about $l/b = 1$ at both small and large angles of attack within the entire range of Froude numbers comprising Sottorf's program. For long plates, on the other hand (large l/b), the agreement was far from satisfactory (curve D in figs. 14 to 16). This might be due in part to the increasing gravity effect with great plate length; then, too, it should be observed that Wagner's theory for the case of long planing surfaces is applicable only to very (infinitely) small angles of attack. And so the discrepancies between theory and experiment could be traced to the fact that the assumption of infinitely small angle of attack did not constitute a sufficiently close approximation for Sottorf's test range.

2. Experiments

The purpose of the experiments was to elucidate these discrepancies between theory and experiment; that is, to separate as far as possible the effect of gravity and that of the finite angle of attack. With this in mind, I made a series of tests with the high-speed carriage in the Prussian Experimental Laboratory for Hydraulics and Ship Design, Berlin, on flat planing surfaces at largest possible Froude numbers; that is, at the highest possible test speed and with the smallest possible plates. (See table I at end of report.) In distinction to Sottorf's tests (reference 3) the peak speed V was raised from 9.5 to 16 meters per second; and the plate width b. reduced from 30 to 15 centimeters, thus raising the highest obtained Froude number $F = V/\sqrt{bg}$ to 2.37 times its value. The experiments with long plates and high load rating, restricted to 6 meters per second speed in Sottorf's test, were considerably extended.

The experimental arrangement, patterned largely after Sottorf set-up, is described later on.

As in Sottorf's experiments, the plates wore left free to trim and loaded with weights (figs. 1 and 22). At the chosen load ratings $\dfrac{R}{\frac{\rho}{2} V^2 b^2} = 0.218, 0.109,$ and

0.0545* (see table I), this assured three groups of tests
(figs. 2 to 4, 14 to 16, and 17 to 19) which, in turn,
were subdivided according to Froude number (speeds) into
test series with constant weight loading but variable cen-
ter-of-gravity position. Table I also indicates the test
series, run with the 15- and 30-centimeter plates. To as-
sure greater accuracy and at the same time afford a check
on Sottorf's measurements, the tests were made - as far as
the experimental set-up allowed - with the 30-centimeter
plate. Because it was occasionally expedient to analyze
the test data in relation to the speed rather than the
Froude number (figs. 2-4, 14-16, and 17-19), and also be-
cause the speeds at equal Froude number are proportional
to the roots of the plate widths, the speed was referred
to one plate width. In the following it was referred and
converted to the 30-centimeter plate (figs. 2-4, 14-16,
and 17-19), the same as Sottorf employed in his tests.

As in Sottorf's case (figs. 1 and 22), our experi-
ments covered:

1. The produced wetted length l of the pressure
    surface;

2. The ensuing angle of attack β of the planing
    surface; and

3. The drag W_Z of the planing surface (push-rod
    force).

The position of the lift resultants (fig. 1 and table
I, columns 6 and 13) and their components normal to the
planing surface $(= R)$ and in the plane of the planing
surface $(= W_R = \text{friction})$ were mathematically established
from G_V and G_H, the plate weight and W_Z; from W_R
followed the coefficient of friction $c_f = \dfrac{W_R}{\dfrac{\rho}{2} V^2\, b\, l}$ (ta-
ble I, columns 8 and 15).

3. Results of Experiments (Airfoil Comparison)

The results are shown in figures 2 to 4, with $1/F^2$,
the reciprocal value of the squared Froude number F as

---

*Corresponding to Sottorf's load ratings $C_B = 0.218$,
0.109, and 0.0545 (reference 3).

abscissa. The speeds converted:for the 30-centimeter
plate are included also. The right-hand side of each one
of the three plots corresponds to low speed (great grav-
ity effect), with the left border $\frac{1}{F}$ = 0 corresponding
to the extreme case of infinitely high speed; that is, the
gravity-free problem. As ordinate, we plotted with the
aid of figures 14 to 16, the experimental angle of attack
β for the assumed l/b in figures 2 to 4. The curves
connecting the individual β values give the angle-of-
attack range for given l/b of the planing surface at
constant lift coefficient c_a.

     Figure 2 illustrates the results for the high load
rating (i.e., large β), and figures 3 and 4, for low load
rating (i.e., small β). Winter's wind-tunnel tests* (ref-
erence 6) - the results of which are reproduced in figure
25 - are also represented by the angles of attack of flat
airfoils at doubled lift coefficients c_a at $\frac{1}{F^2}$ = 0 for
l/b = 1, 2, and 3. The good agreement existing between
airfoil and planing surface test data at large Froude num-
bers, even for great plate lengths and high β (figs. 2 to
4), constitutes the first result of our work; that is,
contrary to the original expectations, the airfoil compar-
ison retains its validity even at larger angles of attack.

     If the gravity (Froude number) and the viscosity ex-
erted no effect on the process, each plotted curve would,
in conformity with the general dynamic law of similitude,
be a straight line β = constant; because for every one of
these curves the plate loading was varied as the square
of the speed. The slope of the curves is, in consequence,
a criterion for the actually existing gravity and viscos-
ity effect.

     The drag W of flat planing surfaces with no allow-
ance for viscosity, is given in figure 1 for given loading
R and angle β with W = R sin β. Figures 2 to 4 show
that W and β increase in part and drop in part with
increasing Froude number; that is, with rising gravity ef-
fect under otherwise identical conditions.

----

*Airfoil investigations made by H. Winter in the wind tun-
nel of the Danzig Technischen Hochschule (chair, Professor
Flügel). These experiments are much more accurate than the
hitherto known experiments with long surfaces by Eiffel
(reference 7).

Before proceeding with the discussion of figures 2 to 4, a few words about the viscosity effect may be to the point. That this effect in the boundary layer is negligibly small on the effective angle of attack, is borne out by the following argument: Suppose a very thin turbulent frictional layer starts to form on the leading edge of the planing surface (fig. 5) which at the end of the plate possesses the velocity distribution according to equation $\frac{\overline{V}}{V} = \left(\frac{y}{\delta}\right)^{1/7}$ (fig. 6), whereby $\overline{V}$ = velocity of potential flow outside of frictional layer (= plate speed), y = distance from plate and $\delta = 0.37 \, l \sqrt[5]{\frac{1}{R}}$ = thickness of frictional layer. Then the thickness δ of the frictional layer at the leading edge, affected by friction while passing by the plate, follows from

$$V \, \delta_1 = \int_{y=0}^{y=\delta} \overline{V} \, dy$$

having recourse to equation $\frac{\overline{V}}{V} = \left(\frac{y}{\delta}\right)^{1/7}$ at $\delta_1 = \frac{7}{8}\delta$ (fig. 6).

Owing to the friction on the plate, the potential flow is deflected through an angle $\Delta \beta_W = \frac{\delta}{8l}$ (fig. 6), which is followed by an increase in effective angle of attack and hence a rise in lift by ΔR. With minor discrepancies the interpretation of the test data gave $\Delta \beta_W = 0.15°$ (table I, column 17). The experimental accuracy for the angle of attack being $\pm 0.1°$, the friction effect may be ignored. Admittedly, the cited change ΔR due to the change in β_W does not exhaust the effect of viscosity on the lift. As on the airfoil, the cumulative lift ΔR of the planing surface is in a well-defined relationship with the friction in the boundary layer. For the two-dimensional airfoil problem, this relationship has been rather well cleared up by Betz (references 8 and 9); but the three-dimensional problem of the long planing surface presents so much greater difficulties, which probably will not be overcome until after exhaustive measurements of the actual velocity distribution in the boundary layer have been made and when it becomes possible to ascertain the cumulative lift ΔR by measurement.

After this digression, we return to our discussion of figures 2 to 4.

According to Wagner's theoretical reasoning, the drag (angle of attack) of wide and short plates and given loading increases with increasing gravity effect (decreasing Froude number). The experiments (figs. 2-4) actually manifest this effect on short plates (at least up to $l/b = 2$) at all load stages. In fact, these short plates disclosed, even at the highost Froude numbers reached in the test, a change in angle of attack (drag) with the Froude number.

As rogards very long plates $\left(\frac{l}{b} = 3\right)$ the gravity appears to have a drag decreasing rather than increasing effect ($\beta = $ approximately constant), according to figures 2 to 4. At least, this holds true for the highest Froude numbers reached in the test, which is in line with Sottorf's results (figs. 2-4). At very low speeds the loading of the planing surfaces is finally borne free from drag by the buoyant lift. But it is precisely the long plates which, in viow of the persistence of the gravity on the short plates at equal Froude numbers, soem to raise the doubt as to whether the tests actually correspond already to the gravity-free problem.

But that this is actually the case is suggested from the airfoil data plotted at $\frac{1}{F^2} = 0$, provided these values themselves are correct and not, perhaps, afflicted with an appreciable orror due to chamfering of the leading and trailing edges, or caused by the conversion of the test data (figs. 26 and 27).

In order to bring out the accord between the planing surface and airfoil data oven more clearly, figure 7 shows the lift coefficients $c_a = \dfrac{R}{\frac{\rho}{2}\,V^2\,b\,l}$ against angle of attack for the three load stages, the region of maximum Froude numbers reached in the test $F = 13.05$ and $F = 3.47$ being shown as shaded area. (It corresponds in figs. 2-4 to the range between $V = 22.6$ and 6 meters per second.) The graph also includes half the lift coefficients c_a of flat planing surfaces with the aid of figure 29. The good agreement extends far beyond that predicted by Wagner for infinitely small angles of attack and includes, in fact, a considorable range of Froude numbers.

This accord between planing surface and airfoil ties in with the following theoretical consideration.

According to the theory of aerodynamics, the lift of an airfoil can be considered as equivalent to a downward motion remaining behind the airfoil in the fluid (fig. 8). The same holds for the planing process in the gravity-free problem.

Then on a long, narrow plate a plane flow may be assumed to exist in the after-region of the plate in the planes perpendicular to the direction of flow. The downward momentum B of the water mass lying between two such planes of distance "one" is $B = V_i m$, whereby $V_i = V \beta$ is the downward velocity of the water at the plate and m the entrained (reduced to V_i) quantity of water. Now since this momentum of the plane flow can equally be assumed to remain unchanged behind the plate, the lift R of the plate can be computed from the momentum theorem at

$$R = B V = V^2 \beta m \qquad (1)$$

The entrained water mass m depends upon the form of the flow. At infinitely small β of the plate the entrained mass $m = m_0$ (or m_0') corresponds to half (or whole) the mass of the circular cylinder with diameter of the plate width b (fig. 9):

On the planing surface	On airfoil
$m_0 = \frac{1}{2} \rho\, b^2\, \frac{\pi}{4}$	$m_0' = \rho\, b^2\, \frac{\pi}{4} \qquad (2)$

For finite β the entrained water mass m of the planing surface corresponds to the contour of the water; for the airfoil, to the form of the vortex surface ((figs. 10 and 11). The vortices shed from the lateral edges of the airfoil appear in the plane flow as spiral vortex areas in the rear region of the airfoil. The form of those contours and vortex surfaces is defined by one independent variable, i.e., t/b, whereby $t = l \beta$ is the depth of the immersed trailing edge of the planing surface and the height of the plate of the airfoil (perpendicular to flow direction) (figs. 10 and 11).

So if μ (or μ' for the airfoil) is the ratio of entrained water mass m at finite β to that at infinitely

small β or, in other words,

On the planing surface	On airfoil	
$m = \mu \, m_0$	$m' = \mu' \, m_0'$	(3)

then μ (and μ') can only be dependent on t/b.

For the lift of this long plate, the following is therefore applicable:

On the planing surface	On airfoil	
$R = \mu \, R_0$	$R' = \mu' \, R_0'$	
$\quad = \mu \, m_0 \, V^2 \, \beta$	$\quad = \mu' \, m_0' \, V^2 \cdot \beta$	
$\quad = \mu \, \dfrac{1}{2} \, \rho \, \dfrac{\pi b^2}{4} \, V^2 \, \beta$	$\quad = \mu' \, \rho \, \dfrac{\pi b^2}{4} \, V^2 \, \beta$	(4)

whereby R_0 and R_0' denote the lift coefficients computed according to the theory for infinitely small β (that is, according to equation (2), fig. 9).

Winter's studies afford a double check on this line of reasoning for the airfoil:

1. Does μ' actually depend on t/b only?

2. Does the result of the airfoil tests for the case of very small immersion depth (i.e., small β) with $\mu' = 1$ agree with equation (4)?

Note 1:　Figure 12 gives the lift ratio $\mu' = \dfrac{A'}{A_0'} = \dfrac{m'}{m_0'}$

for various airfoil lengths (parameter) and various β (= 5°, 10°, and 15°) against $\dfrac{t}{b} = \dfrac{l\beta}{b}$. The individual values of μ were obtained from

$$\mu' \, \rho \, \frac{\pi b^2}{4} \, V^2 \, \beta = c_a \, \frac{\rho}{2} \, V^2 \, b \, l$$

$$\mu' = \frac{2}{\pi} \, \frac{l}{b} \, \frac{c_a}{\beta}$$

by having recourse to Winter's data $c_a \left(\beta, \frac{l}{b}\right)$ (solid curves, fig. 29). It is seen – and this is a further result of this study – that all these test points for $\frac{l}{b} \geq 2$ lie fairly well on one curve; that is, that the lift ratio μ' is in fact dependent on t/b only.

Note 2: The curve laid through the test points can be extended to the left as far as $\frac{l}{b} = 0$ and readily carried to point $\mu' = 1$. That this is fairly exact for airfoils with $\frac{l}{b} \geq 1$ is also seen from figure 29, where the dashed straights $c_{a_0} \left(\beta, \frac{l}{b}\right)$ obtained from equation (4) with $\mu' = 1$, represent fairly accurately the tangents to the curve $c_a (\beta, l/b)$ at point $\beta = 0$. The minor discrepancies from the mean curve are – excepting experimental inaccuracies – for short plates, in part, perhaps, attributable to the fact that the premise of plane flow in the region of the trailing edge is not completely fulfilled. Then, too, Winter's experiments, unfortunately, do not give a complete picture of the forces on plane airfoils. The test plates were slightly cambered at leading and trailing edges, which at very small β revealed itself as a disturbing influence.

The comparison (figs. 2-4) discloses that at finite β and large F the tests for the planing surface lift yield 50 percent of the airfoil lift. This – the third result of the study – means that, within the bounds of experimental accuracy, the reduced masses for the planing surface are – even at finie β – half as large as for the airfoil.

Whence follows the fourth fact, to wit: the lift conditions of planing surfaces do not change linearly with β (fig. 29). And this is the reason why an attempt to develop a theory for the long plate conformably to Blenk's (reference 10) theory for the short plate, appears to hold out little promise.

The results of the last consideration lend point to a deduction about the magnitude of lift of long, longitudinally curved planing surfaces. Even these cambered planing

surfaces reveal in the region of the planing edge a plane
flow which should not be much unlike that on the flat plan-
ing surface (fig. 13). The total lift of such a planing
surface should therefore be just about as high as that of
a flat planing surface with the same t/b, and further-
more, this relation should hold for infinitely small as
well as for finite β. Unfortunately, Sottorf's experi-
ments do not lend themselves to such a check on account of
the low F in the experiments with curved plates.

Mathematical Treatment of Figure 12

1	2	3	4	5	6	7	8	9	10
	$\beta = 5°$			$\beta = 10°$			$\beta = 15°$		
l/b	c_a/β	μ'	$\frac{t}{b}=\frac{l}{b}\beta$	c_a/β	μ'	$\frac{t}{b}=\frac{l}{b}\beta$	c_a/β	μ'	$\frac{t}{b}=\frac{l}{b}\beta$
1.	1.9	1.21	0.087	2.07	1.32	0.174	2.24	1.43	0.261
2	1.26	1.61	.174	1.56	1.98	.348	1.76	2.24	.522
3	.94	1.80	.261	1.23	2.34	.522	1.45	2.76	.783
7.45	.64	3.04	.548	.86	4.10	1.295	1.02	4.86	1.945
30.0	.31	6.01	2.61	.49	9.29	5.22	.65	12.03	7.83

$\mu' = \frac{2}{\pi}\frac{l}{b}\frac{c_a}{\beta}$ μ' is plotted against $\frac{t}{b}$; $\frac{c_a}{\beta}$ was charted from
figure 29.

Figures 14 to 16 contain the data for the flat planing
surface in the conventional manner (reference 2, fig. 14),
with the ensuing β plotted against l/b for the three
load stages. The individual curves are the result of join-
ing the test points for the different speeds (Froude num-
bers).

Curve A represents the test data for the highest Froude
number reached in the test (figs. 2-4) and consequently,
approximates the conditions encountered with the gravity-
free problem.

Curve B, obtained from Winter's airfoil studies (figs.
2-4, points at $\frac{1}{F^2} = 0$) is fairly coincident with curve A.

Curve C is obtained conformably to Prandtl's airfoil theory for the infinitely short airfoil in frictionless, gravity-free motion with consideration of the finite β in conjunction with equations (10) and (18) of reference 2. The calculation given in table II was made as follows: The value κ (table II, column 3) was computed from figure 18, reference 2, for several arbitrarily assumed effective β_w (table II, column 1), after which the value

$$\frac{l}{b} = \frac{R}{\frac{\rho}{2} V^2 b^2} \frac{1}{\kappa \pi \beta_w} \quad \text{was obtained for each } \beta_w \text{ from } R =$$

$\kappa \frac{\pi}{2} \rho V^2 \beta_w b l$ (reference 2, equation (10)) for the three load stages (table II, columns 4, 6, and 8). Against these values as abscissa, we then plotted the value $\beta = \beta_w + \beta_1$ (table II, columns 5, 7, and 9) for the three load stages as ordinate. The fact that this curve actually coincides at certain load stages with the test data for long plates, is nothing more than mere chance. At still lower load stage the test values would lie above this curve.

Curve D, which is valid for the long plate in the extreme case of infinitely small β was arrived at as follows: For flat planing surfaces and very (infinitely) small β, it is $\dfrac{\beta_1}{\beta} = \dfrac{W_1}{W}$. From $\beta_1 = \dfrac{4R}{\pi \rho V^2 b^2}$ follows

$\beta = \dfrac{1}{W_1/W} \dfrac{4R}{\pi \rho V^2 b^2}$ (reference 2, equation (22), whereby

$R = A$) where W_1/W is a function of l/b (fig. 9, reference 2). The mathematical treatment is seen from table III. When the plates are long the curve manifests a marked discrepancy from the experimental results.

This departure of curve D from the experimental results, the explanation of which formed the object of this study, does not rest on the gravity effect but rather upon the fact that the lift conditions do not change linearly with the angle of attack.

Figures 17 to 19 give the position of the lift resultant l_p/l against l/b (table I, columns 6 and 13) for the flat planing surface at the three load stages. The speeds plotted in the upper chart again refer to the 30-centimeter plate. The corresponding curves (i.e., for load stage twice as high) from Winter's airfoil tests

(figs. 28 and 30) are also given for comparison. The partially marked discrepancies from the curve obtained in airfoil tests are perhaps difficult to explain; and they probably constitute the chief cause of the experimental accuracy, for slight, unavoidable errors in loading or friction in the test lay-out - insignificant as far as the other measurements (β and l) are concerned - exerted, on account of the great lever arms, a great influence on the determination of the moment about the trailing edge and through it, upon the position of the center of pressure. More accurate measurements of the position of the lift resultant on planing surfaces are desirable in order to remove the existing doubts.

TABLE II. Mathematical Treatment for Curve C (figs. 14-16)

1	2	3	4	5	6	7	8	9
$\beta_W = \beta - \beta_1$			$\dfrac{R}{\frac{\rho}{2}V^2 b^2} = 0.218$			$= 0.109$		$= 0.0545$
			$\beta_1 = 8°$			$= 4°$		$= 2°$
degree	arc	κ	l/b	$\beta°$	l/b	$\beta°$	l/b	$\beta°$
0.3	0.00523	0.99	13.4	8.3	6.7	4.3	3.35	2.3
.5	.00873	.983	8.08	8.5	4.04	4.5	2.02	2.5
.75	.0131	.978	5.42	8.75	2.71	4.75	1.36	2.75
1.0	.0175	.97	4.08	9.0	2.04	5.0	1.02	3.0
1.5	.0262	.957	2.77	9.5	1.38	5.5	.69	3.5
2.0	.0349	.944	2.11	10.0	1.06	6.0	.53	4.0
3.0	.0524	.918	1.44	11.0	.72	7.0	.36	5.0
4.0	.0698	.895	1.11	12.0	.56	8.0	.28	6.0
6.0	.1047	.85	.78	14.0	.39	10.0	.19	8.0
8.0	.1396	.805	.618	16.0	.31	12.0	.15	10.0
10.0	.1745	.765	.52	18.0	.26	14.0	.13	12.0

$l/b = \dfrac{R}{\frac{\rho}{2}V^2 b^2}\ \dfrac{1}{\kappa \pi \beta_W}$; obtained from $R = \kappa \dfrac{\pi}{2}\rho V^2 \beta_W\, b\, l$

(reference 2, equation 10)

$\beta_1 = \dfrac{4R}{\pi \rho V^2 b^2} = \dfrac{R}{\frac{\rho}{2}V^2 b^2}\ \dfrac{2}{\pi}$ (reference 2, equation 18)

κ (reference 2, fig. 18) $\beta = \beta_W + \beta_1$

TABLE III. Mathematical Treatment for Curve D (figs. 14-16)

1	2	3	4	5
			β^o	
			for $\dfrac{R}{\frac{\rho}{2} V^2 b^2} =$	
l/b	W_1/W	$= 0.218$	$= 0.109$	$= 0.0545$
1	0.55	14.54	7.27	3.63
1.5	.555	14.4	7.2	3.6
2	.545	14.66	7.33	3.66
2.5	.53	15.1	7.55	3.77
3	.516	15.5	7.75	3.88
3.5	.512	15.62	7.81	3.90

W_1/W (reference 2, fig. 9)

$$\beta = \frac{1}{W_1/W} \frac{4R}{\pi \rho V^2 b^2} = \frac{1}{W_1/W} \frac{R}{\frac{\rho}{2} V^2 b^2} \frac{2}{\pi} \quad \text{(reference 2, equation 22)}$$

4. Recapitulation

In the endeavor to adduce additional data on the processes on planing surfaces, we attacked the problem in two ways: complementary tests and theoretical deductions.

As regards short, flat planing surfaces, the result was as theoretically anticipated: the gravity has a drag increasing effect.

For long, flat planing surfaces, it was found that:

1. The airfoil comparison retains, contrary to the original expectations, at large Froude numbers, its validity even for greater angles of attack;

2. The lift conditions for planing surfaces of any length can be expressed by one single curve $\mu' = \mu'\left(\dfrac{l}{b}\right)$,   even with finite angle of attack

3. Even at finite angle of attack, the reduced mass is half as great as for the airfoil;

·4.   Contrary to the original expectations, the lift
      conditions do not change linearly with the
      angle of attack.

The gravity-free problem thus appearing to be cleared
up to some extent, the effect of gravity on the angle of
attack following the drop in pressure as a result of the
gravity - or what is equivalent to a rotation of the flow
picture - as well as on the lift due to buoyant lift, can
now be more clearly isolated and studied (reference 2, pp.
212-215). This might be important for future experimental
and theoretical studies.

PART II

1. Experimental Arrangement (figs. 20-22)

A detailed description of the high-speed carriage and
of the drag-recording instruments can be found in refer-
ence 11. Suffice it to note here that the drag-recording
equipment is so controlled by electric contact that the
push rod always remains horizontal. The front and sides
of the carriage are fitted with windshields as in Sottorf's
later studies (references 4 and 5). Trial runs revealed
the necessity for damping devices fore and aft of the
plate to dampen the plate motions.

As distinct from Sottorf's use of wooden plates with
inserted glass strips, our plates were of plate glass 7
and 12 millimeters thick, fastened by countersunk screws
to Lautal supports. The holes in the plates, necessary
for mounting, were plugged with sealing wax. For the de-
termination of the wetted length the glass plates carried
a scale counting from the trailing edge.

2. Test Procedure

The tests followed a systematic schedule including all
data on magnitude and distribution of the loading weights.
This reduced the number of runs necessary for exploring
the questionable regions to a minimum. The plate was left
free to trim during the run. The test data for given
amount and position of loading included:

1.   The ensuing wetted length l of the pressure
     surface;

2. The ensuing angle of attack β of the planing surface;

3. The drag of the planing surface W_Z (push-rod effort) (fig. 1).

Angle β was measured by recording the forward and rear trims. The wetted length l (= area of pressure surface divided by plate width b) was obtained from photographs of the surface pushed by the water, the pictures being taken by a camera mounted on the planing surface, the shutter being released mechanically at a certain point during the run. To assure a check on the constancy of the wetted length during the run, apart from the trim record, three photographs were taken on one plate at time intervals equivalent to about 6 meters running distance. In fact the photographs disclose two - and at times three - contours close to each other, so that the reading may be considered to be fairly reliable (figs. 23-25). Speed and position of plate being practically unchanged during the actual recording period, reduces the conditions of the tests to those of a stationary flow.

The upright digits in figures 23-25 give the numbers of the run. They corresponded, for instance, with numbers 50, 52, and 58 on figures 23-25, to test numbers 32, 13, and 12 of the test program in table I.

The interval between tests averaged about 20 minutes and was long enough to practically return the water to a state of rest.

3. Evaluation of the Experiments

This time interval was employed for evaluating the tests - i.e., for developing the films, in order to ascertain the wetted length, obtain the angle of attack from the front and rear trim record, read the horizontal push-rod force from the diagram, and complete the actual running speed, from which data and the applied loading weights the magnitude, position, and direction of the lift resultant were obtained. In the event that minor deviations from the contemplated speed and from the intended plate normal force had caused a departure from the intended load stage, this fact was allowed for by a correction in the angle of attack. For in gravity-free motion the angle of attack reacts the same as the load stage, whether the planing surface is short (reference 2, equation 19) or long (reference 2, equation 21).

4. Experimental Accuracy

As regards the accuracy of the test values, it may be stated that the errors in the determination of the angle of attack are less than 1/10 degree, and that the actually attained speed was, at the most, 1.5 percent at variance with the purposed speed. The force measurement was practically free from error, although occasionally some very small, inevitable waves in the tank made the measurement of the wetted length on short plates quite difficult, particularly as an error in reading here of even a few millimeters, spelled an appreciable error in the determination of the position of the lift resultants. Elastic strains of the balance were allowed for in the evaluation.

PART III

Note on Winter's Experiments

Winter's test data are reproduced in figures 26 and 27. Having beveled off, for the purpose of better adherence of flow, the leading and trailing edges of the plates, equivalent in effect to a plate curvature, the curves do not pass through the zero point. The effect of this initial curvature was neutralized by placing the abscissa through the point of intersection of the curves with the ordinate axis (figs. 28 and 29). The dashed lines in figure 29 give the $c_a-\beta$ values according to the theory for very (infinitely) small angle of attack. They were obtained from

$$\rho \, \frac{\pi b^2}{4} \, V^2 \, \beta = c_a \, \frac{\rho}{2} \, V^2 \, b \, l$$

from which follows

$$\frac{c_a}{\beta} = \frac{\pi}{2} \, \frac{1}{l/b}$$

The $c_m-\beta$ values of figure 28, referred to the leading edge of the plate, were converted for the planing surface analysis to the trailing edge as reference point (fig. 30). Figures 29 and 30 show the curves on which the planing surface evaluation had been based.

Translation by J. Vanier,
National Advisory Committee
for Aeronautics.

REFERENCES

1. Wagner, H.: Über Stoss- und Gleitvorgänge an der Oberfläche von Flüssigkeiten. Z.f.a.M.M., Bd. 12, (1932), S. 193-215.

2. Wagner, H.: Über das Gleiten von Wasserfahrzeugen. Jb. schiffbautechn. Ges. (1933), S. 205-227.

3. Sottorf, W.: Experiments with Planing Surfaces. T.M. No. 661. N.A.C.A., 1932.

4. Sottorf, W.: Experiments with Planing Surfaces. T.M. No. 739, N.A.C.A., 1934.

5. Sottorf, W.: Scale Effect of Model in Seaplane-Float Investigations. T.M. No. 704, N.A.C.A., 1933.

6. Winter, H.: Flow Phenomena on Plates and Airfoils of Short Span. T.M. No. 798, N.A.C.A., 1936.

7. Eiffel, G.: Der Luftwiderstand und der Flug. Deutsche Übersetzung im Verlag Richard Carl Schmidt & Co., Berlin W 62, 1912.

8. Betz, A.: Theoretische Berechnung von Tragflügelprofilen. Z.F.M., Bd. 24 (1933), S. 437.

9. Stüper, I.: Reduction of Lift of a Wing Due to Its Drag. T.M. No. 781, N.A.C.A., 1935.

10. Blenk, H.: Der Eindecker als tragende Wirbelfläche. Z.f.a.M.M., Bd. 5 (1925), S. 36-47.

11. Weitbrecht, H. M.: Einrichtung zum Schleppen von Modellen mit hohen Geschwindigkeiten, Z.V.D.I., Bd. 76 (1932), S. 1119-1122.

* > 10% gravity

Table 1.- Test program and results.

O = moment-reference point

$\mathbf{F} = \dfrac{V}{\sqrt{b \cdot g}}$ = Froude number

$\mathbf{R} = \dfrac{Vl}{\nu}$ = Reynolds Number

$M = R \cdot l_p$

$c_f = \dfrac{W_u}{\frac{\varrho}{2} V^2 F}$ = coefficient of friction

$\dfrac{R}{\frac{\varrho}{2} v^2 b^2} = 0,218$

$b = 15$ cm

No. test	β°	l cm	l cm	M cm kg	l_p/l	R·10⁻⁴	c_f

b = 30 cm

β°	l cm	l cm	M cm kg	l_p/l	R·10⁻⁴	c_f	l/√M (λ=0,37)	Δβ_w = λ/8l

$V = 6$ m/s $R = 36$ kg $\mathbf{F} = 3,47$

1									11,55	36,5	5,78	945	0,705	2,19	0,00201	0,734	0,00251
2	A								14,0	28,0	3,52	686	0,71	1,56	0,00078	0,560	0,00269
3									19,2	16,0	1,86	406	0,711	0,96	-0,00185	0,379	0,00296

$V = 7,5$ m/s $R = 50,25$ kg $\mathbf{F} = 4,33$

4									11,45	36,0	4,60	1457	0,706	2,70	0,00140	0,694	0,00241
5									13,85	28,0	3,35	1060	0,706	1,95	0,00074	0,535	0,00257
6									19,85	17,0	1,86	602	0,644	1,28	-0,0023	0,393	0,00289

$V = 6,718$ m/s $R = 11,3$ kg $\mathbf{F} = 5,5$

$V = 9,5$ m/s $R = 90,4$ kg $\mathbf{F} = 5,5$

*7	6,96	50,0	6,07	457	0,712	3,36	0,00340								0,915	0,00229
*8	7,38	40,0	5,27	379	0,72	3,10	0,00310								0,860	0,00234
9	8,98	30,0	4,10	262	0,736	2,06	0,00266								0,622	0,00254
10	10,28	23,0	3,08	191	0,718	1,55	0,00242								0,495	0,00269
11	12,10	15,7	2,16	123	0,689	1,06	0,00106								0,363	0,00289
12	16,33	10,0	1,25	85	0,724	0,67	-0,00144								0,253	0,00316

$V = 8,485$ m/s $R = 18$ kg $\mathbf{F} = 6,93$

$V = 12$ m/s $R = 144$ kg $\mathbf{F} = 6,93$

13	7,35	45,5	5,12	606	0,729	3,36	0,00289								0,813	0,00223
14	8,83	30,5	3,68	400	0,725	2,68	0,00190								0,591	0,00242
15	9,81	23,6	3,05	311	0,723	1,90	0,00134								0,483	0,00257
16	12,38	15,2	2,00	190	0,684	1,29	-0,000975								0,335	0,00275
17	16,55	9,8	1,20	125	0,695	0,83	-0,00311								0,238	0,00304

$V = 11,314$ m/s $R = 32$ kg $\mathbf{F} = 9,25$

$V = 16$ m/s $R = 256$ kg $\mathbf{F} = 9,25$

18	7,32	44,0	5,3	1066	0,742	4,07	0,00318								0,750	0,00213
19	8,5	31,0	4,0	750	0,748	3,51	0,00275								0,565	0,00228
20	9,18	24,8	3,23	600	0,750	2,81	0,00254								0,474	0,00239
21	12,48	14,6	2,1	355	0,776	1,65	0,00125								0,307	0,00263
22	14,72	10,8	1,25	245	0,695	1,22	-0,00138								0,244	0,00282

$V = 16$ m/s $R = 64$ kg $\mathbf{F} = 13,05$

$V = 22,6$ m/s $R = 512$ kg $\mathbf{F} = 13,05$

23	7,26	46,0	5,35	2169	0,737	7,35	0,00290								0,725	0,00197
24	7,18	46,5	5,05	2162	0,747	7,45	0,00318								0,728	0,00196
25	8,9	29,0	3,58	1359	0,735	4,63	0,00234								0,501	0,00216
26	9,95	21,0	2,82	979	0,734	3,36	0,00097								0,385	0,00229
27	11,98	14,6	2,1	705	0,758	2,33	-0,00088								0,289	0,00248
28	16,4	9,6	1,29	419	0,689	1,54	-0,00688								0,206	0,00268
29	17,07	9,0	1,5	480	0,734	1,44	-0,00486								0,196	0,00272

$\dfrac{R}{\frac{\varrho}{2} v^2 b^2} = 0,100$

$V = 8,485$ m/s $R = 9$ kg $\mathbf{F} = 6,93$

$V = 12$ m/s $R = 72$ kg $\mathbf{F} = 6,93$

30	4,18	46,0	2,76	318	0,772	3,8	0,00342								0,826	0,00222
31	4,26	45,5	2,92	318	0,77	3,86	0,00321								0,813	0,00222
32	5,0	32,0	2,26	230	0,783	2,72	0,00304								0,617	0,00241
33	4,92	32,5	2,35	229	0,77	2,76	0,00286								0,623	0,00239
34	5,42	25,5	1,94	172	0,741	2,16	0,00319								0,513	0,00251
35	6,51	16,5	1,25	108	0,718	1,4	0,00355								0,361	0,00273
36	6,46	16,2	1,21	108	0,732	1,37	0,00417								0,357	0,00275
37	7,45	12,0	0,92	74	0,674	1,02	0,00324								0,281	0,00293

Table 1.- Continued

b = 15 cm

Vers. Nr.	β° l/l'	l cm λ	l' cm	M cm kg	l_p/l	R·10⁻⁴	c_f

b = 30 cm

β° l'/l'	l' cm	l cm	M cm kg	l_p/l	R·10⁻⁴	c_f	l/√M (λ=0,37)	Δβ_w = λ/8l

$V = 11,314$ m/s $R = 16$ kg $\mathbf{F} = 9,25$

$V = 16$ m/s $R = 128$ kg $\mathbf{F} = 9,25$

38	4,18	47,5	3,15	594	0,773	5,40	0,00372								0,795	0,00209
39	4,23	48,0	2,91	592	0,765	5,43	0,00342								0,900	0,00209
40	5,03	28,5	2,04	353	0,782	3,22	0,00335								0,527	0,00231
41	5,35	22,5	1,71	301	0,831	2,64	0,00304								0,438	0,00243
42	6,26	15,0	0,92	198	0,817	1,70	0,00298								0,316	0,00263
43	7,87	10,0	0,72	118	0,745	1,13	0,00173								0,228	0,00285
44	7,77	10,2	0,80	121	0,745	1,15	0,00153								0,233	0,00285

$V = 16$ m/s $R = 32$ kg $\mathbf{F} = 13,05$

$V = 22,6$ m/s $R = 256$ kg $\mathbf{F} = 13,05$

45	4,23	50,0	3,1	1233	0,768	8,0	0,00340								0,774	0,00193
46	5,0	26,5	1,87	691	0,817	4,23	0,00430								0,485	0,00220
47	5,07	26,0	1,88	688	0,827	4,16	0,00422								0,458	0,00220
48	5,25	22,0	1,53	595	0,844	3,52	0,00392								0,402	0,00228
49	6,13	14,5	1,0	393	0,847	3,32	0,00386								0,267	0,00230
50	7,42	9,5	0,67	273	0,894	1,52	0,00130								0,204	0,00268
51	7,52	9,5	0,58	272	0,892	1,52	0,00160								0,204	0,00268

$\dfrac{R}{\frac{\varrho}{2} v^2 b^2} = 0,0545$

$V = 6$ m/s $R = 9$ kg $\mathbf{F} = 3,47$

52	3,38	36,5	1,15	258	0,776	2,19	0,00328								0,734	0,00251
53	3,9	26,3	0,63	182	0,760	1,58	0,00342								0,563	0,00267
54	5,06	15,8	0,22	108	0,754	0,95	0,00275								0,375	0,00297

$V = 7,5$ m/s $R = 14,06$ kg $\mathbf{F} = 4,33$

55	3,39	36,0	1,0	396	0,78	2,70	0,00337								0,694	0,00241
56	3,85	25,2	0,65	280	0,778	1,89	0,00300								0,515	0,00255
57	4,92	16,0	0,12	165	0,728	1,2	0,00276								0,361	0,00282

$V = 9,5$ m/s $R = 22,6$ kg $\mathbf{F} = 5,5$

*68	2,26	89,0	2,54	1541	0,76	8,45	0,00300								1,360	0,00191
59	3,96	58,5	1,69	1061	0,798	5,55	0,00297								0,971	0,00207
60	2,99	44,5	1,17	816	0,811	4,23	0,00320								0,780	0,00219
61	3,56	30,5	0,86	556	0,794	2,90	0,00333								0,579	0,00247
62	4,25	19,5	0,27	344	0,785	1,85	0,00287								0,403	0,00259

$V = 12$ m/s $R = 36$ kg $\mathbf{F} = 6,93$

63	2,43	87,0	2,55	2436	0,776	10,5	0,00300								1,272	0,00183
64	2,75	58,5	1,69	1701	0,784	7,2	0,00310								0,950	0,00198
65	2,95	48,0	1,42	1350	0,779	5,76	0,00310								0,793	0,00207
66	3,43	31,0	0,71	885	0,790	3,72	0,00310								0,557	0,00225
67	4,06	19,5	0,24	575	0,880	2,34	0,00327								0,386	0,00247

$V = 11,314$ m/s $R = 8$ kg $\mathbf{F} = 9,25$

$V = 16$ m/s $R = 64$ kg $\mathbf{F} = 9,25$

68	2,35	48,5	1,77	312	0,805	5,50	0,00328								0,808	0,00208
69	2,32	40,0	1,56	312	0,848	5,08	0,00362								0,781	0,00213
70	2,60	32,0	1,21	222	0,863	3,62	0,00358								0,580	0,00227
71	2,85	25,5	0,99	174	0,847	2,88	0,00356								0,484	0,00237
72	3,13	20,0	0,84	135	0,835	2,26	0,00336								0,396	0,00248
73	3,73	10,7	0,28	79	0,916	1,21	0,00321								0,242	0,00289
74	3,84	10,6	0,26	80	0,942	1,20	0,00383								0,239	0,00282

$V = 16$ m/s $R = 16$ kg $\mathbf{F} = 13,05$

$V = 22,6$ m/s $R = 128$ kg $\mathbf{F} = 13,05$

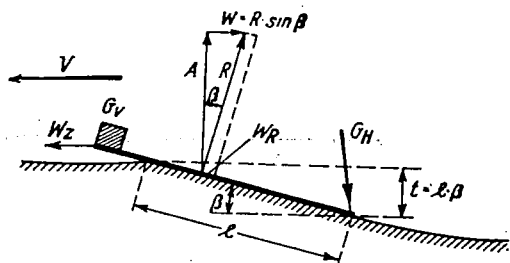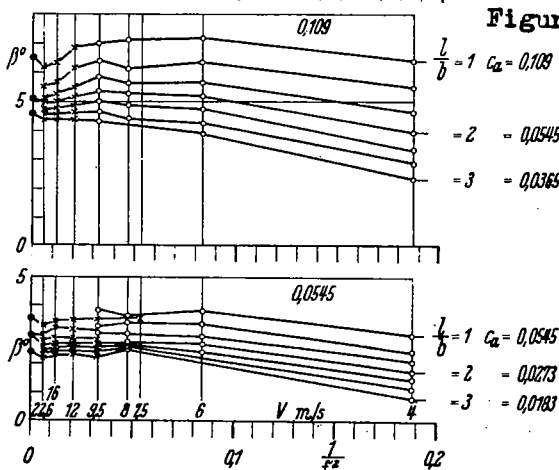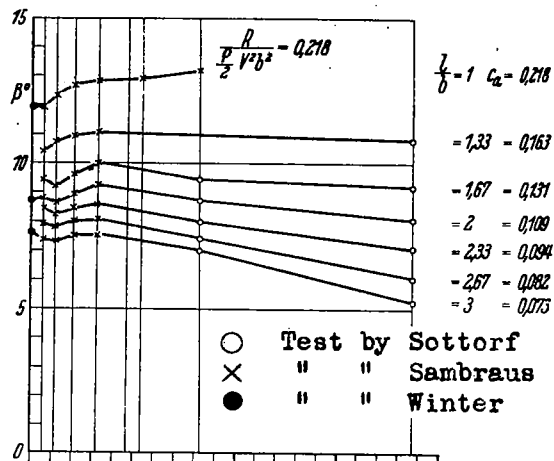| 75 | 2,34 | 46,0 | 1,57 | 633 | 0,850 | 7,35 | 0,00380 | | | | | | | | 0,725 | 0,00197 |
76	2,21	45,0	1,75	636	0,872	7,20	0,00400								0,712	0,00196
77	2,64	29,5	1,13	422	0,888	4,72	0,00417								0,505	0,00214
78	2,93	21,0	0,83	293	0,856	3,36	0,00418								0,385	0,00229
79	3,31	15,0	0,51	227	0,940	2,40	0,00441								0,295	0,00246
80	3,65	11,0	0,33	178	1,010	1,76	0,00606								0,230	0,00261

Table 1

Figure 1.- Test quantities used in experiment. G_V = forward planing surface loading. G_H = rear planing surface loading.

$$\delta = 0.37 \cdot \ell \sqrt[5]{\frac{1}{R}} \qquad \frac{\overline{V}}{V} = \left(\frac{y}{\delta}\right)^{\frac{1}{7}}$$
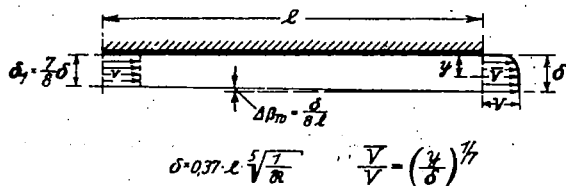
Figure 6.- Effective angle of attack enlarged by $\Delta\beta_w$ as result of turbulent flow on the planing surface.

$$\frac{R}{\frac{\rho}{2}V^2 b^2} = 0.218$$
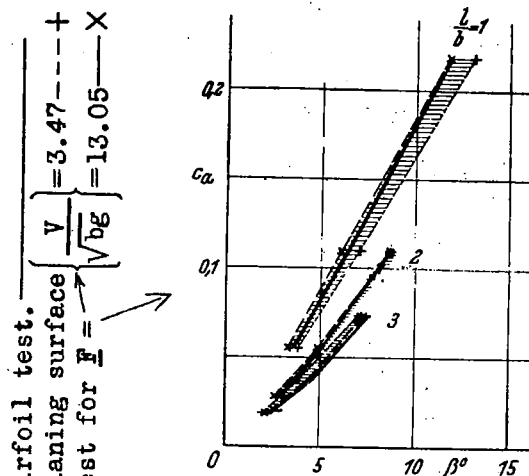
$\frac{l}{b} = 1$	$c_a = 0.218$
$= 1.33$	$= 0.163$
$= 1.67$	$= 0.131$
$= 2$	$= 0.109$
$= 2.33$	$= 0.094$
$= 2.67$	$= 0.082$
$= 3$	$= 0.073$

○ Test by Sottorf
× " " Sambraus
● " " Winter

Figures 2,3,4.- Test data for different load edges.

| 0.109 |
$\frac{l}{b} = 1$	$c_a = 0.109$
$= 2$	$= 0.0545$
$= 3$	$= 0.0365$

| 0.0545 |
$\frac{l}{b} = 1$	$c_a = 0.0545$
$= 2$	$= 0.0273$
$= 3$	$= 0.0183$

$$\delta = 0.37 \cdot \ell \sqrt[5]{\frac{1}{R}}$$

$$\frac{\overline{V}}{V} = \left(\frac{y}{\delta}\right)^{\frac{1}{7}}$$
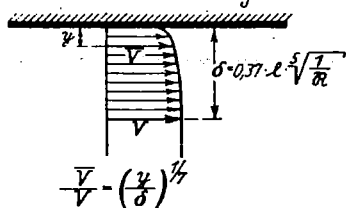
Figure 5.- Velocity distribution of turbulent flow at planing surface.

Airfoil test. Planing surface test for $\mathbf{F} = \left. \frac{V}{\sqrt{bg}} \right\{ \begin{array}{l} = 3.47 \\ = 13.05 \end{array}$

Figure 7.- c_a against β for different $\mathbf{F}$ compared with Winter's airfoil measurements.
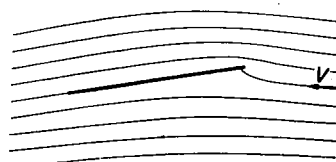
Figure 8.- Flow around flat airfoil.

Planing surface   Airfoil

$$m_o = \frac{1}{2}\rho \, b^2 \frac{\pi}{4} \qquad m'_o = \rho \, b^2 \frac{\pi}{4}$$
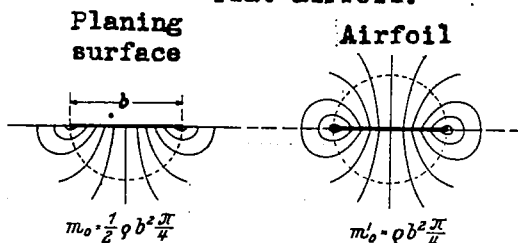
Figure 9.- Flow pattern perpendicular to direction of flow on long planing surface and airfoil.

Planing surface
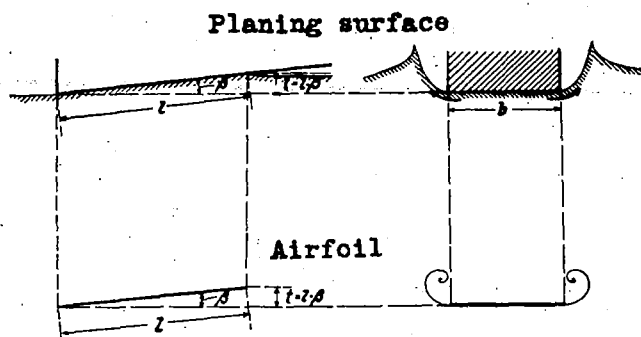
Airfoil

Figures 10,11.- Water contour on planing
surface and vortex sur-
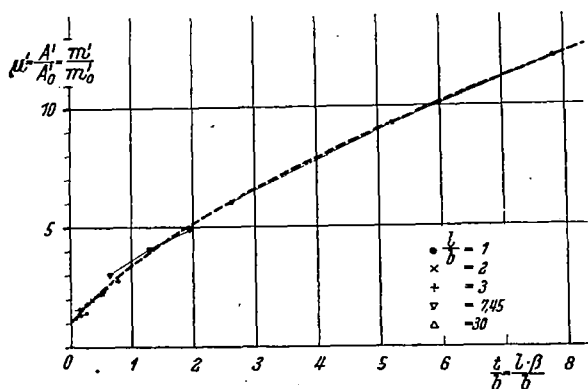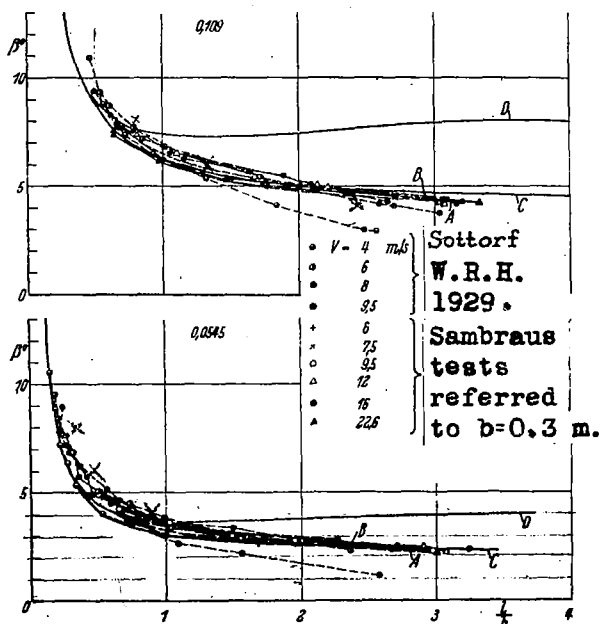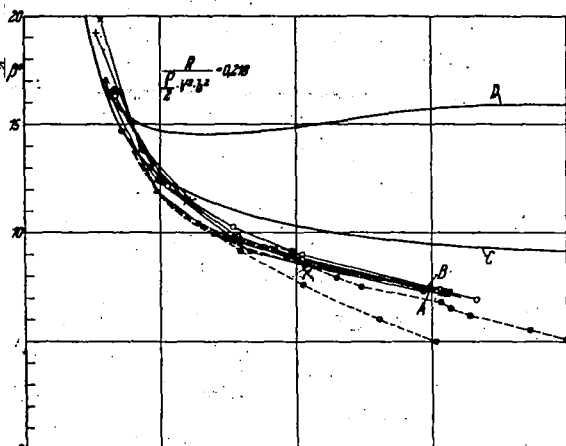face on airfoil in a section perpendicu-
lar to flow direction.

$$\mu' = \frac{A'}{A_0'} = \frac{m'}{m_0'}$$

	$\frac{l}{b}$
●	= 1
×	= 2
+	= 3
▽	= 7.45
△	= 30

$$\frac{t}{b} = \frac{l \cdot \beta}{b}$$

Figure 12.- Calculation and chart
of lift ratio μ' against
t/b for different β and aspect ra-
tios.

$$\frac{p}{\frac{\rho}{2} \cdot v^{2} \cdot b^{2}} = 0.218$$

0.109

0.0545

	$v = 4$ m/s	Sottorf
●	6	W.R.H.
●	8	1929
●	9.5	
+	6	Sambraus
×	7.5	tests
○	9.5	
△	12	referred
●	15	to b=0.3 m.
▲	22.6	

Figures 14,15,16.- Test data for
different load
stages against l/b.
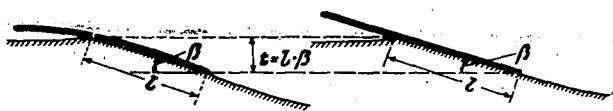
Figure 13.- Flow past flat and curved
planing surface.

$t = l \cdot \beta$

$V = 4$ m/sec
$= 6$ "
$= 7.5$ "
$= 9.5$ "
$= 12$ "
$= 16$ "
$= 22.6$ "
——— Airfoil test

$$\frac{R}{\frac{\varrho}{2}\cdot V^2\cdot b^2} = 0.218$$

$$\frac{R}{\frac{\varrho}{2}\cdot V^2\cdot b^2} = 0.109$$

$$\frac{R}{.\frac{\varrho}{2}\cdot V^2\cdot b^2} = 0.0545$$
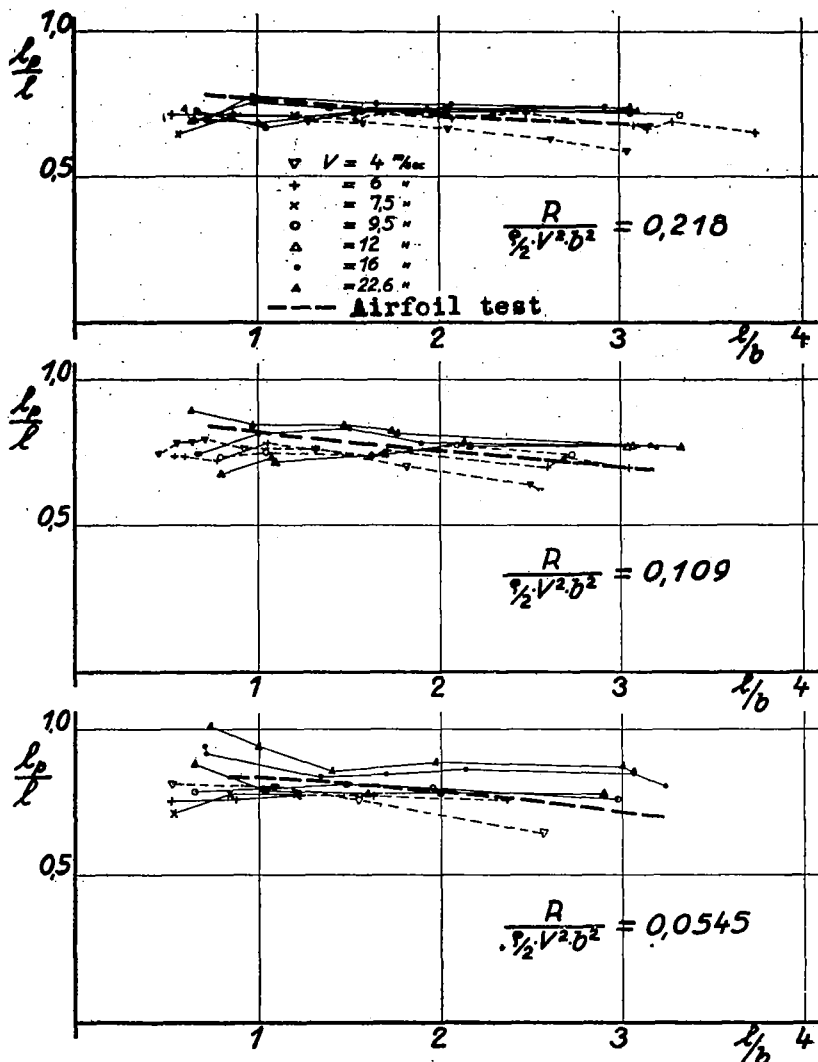
Figures 17,18,19.- Position of lift resultant(l_p/b) against aspect ratio(l/b).

Direction of run
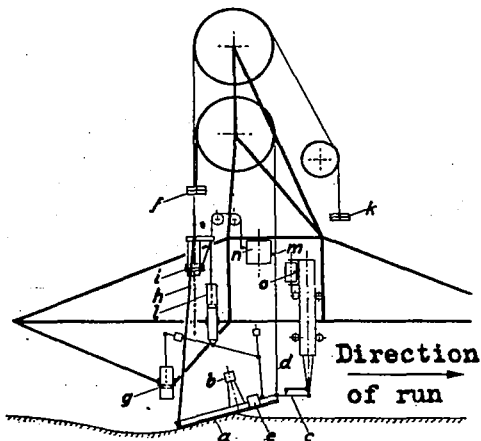
a, Glass plate with holder.
b, Camera.
c, Horizontal push rod with electric
   contact.
d, Forward suspension.
e,   "   loading(weight holder).
f,   "   unloading.
g,   "   damping.
h, Rear suspension(push rod).
i,   "   loading.
k,   "   unloading.
l,   "   damping.
m, Front trim record.
n, Rear   "   " .
o, Drag record.

Figure 22.- Experimental set-up with high-speed carriage.
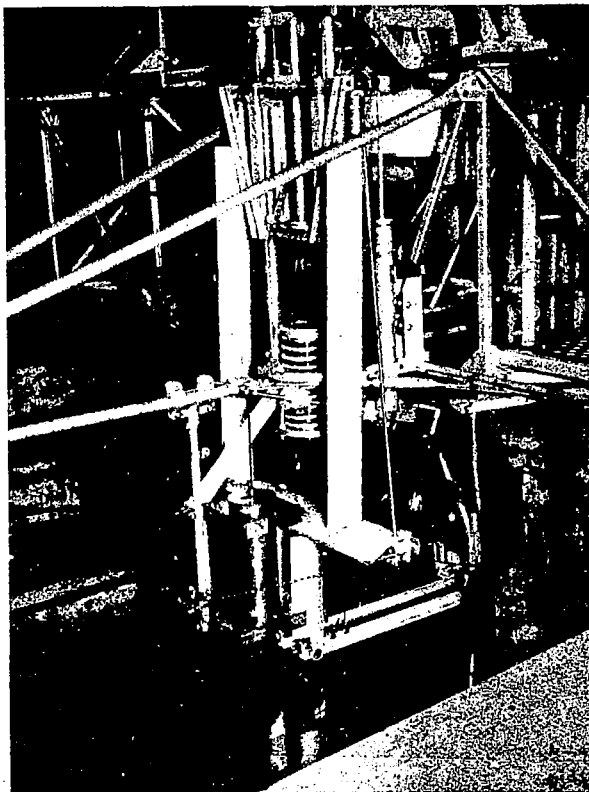
Figure 20.- Installation of planing surface.
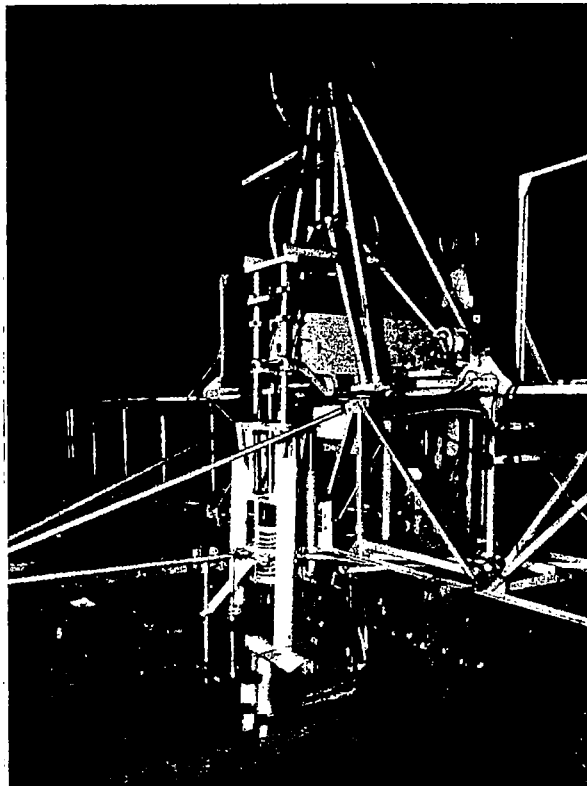
Figure 21.- Experimental set-up with high-speed carriage.

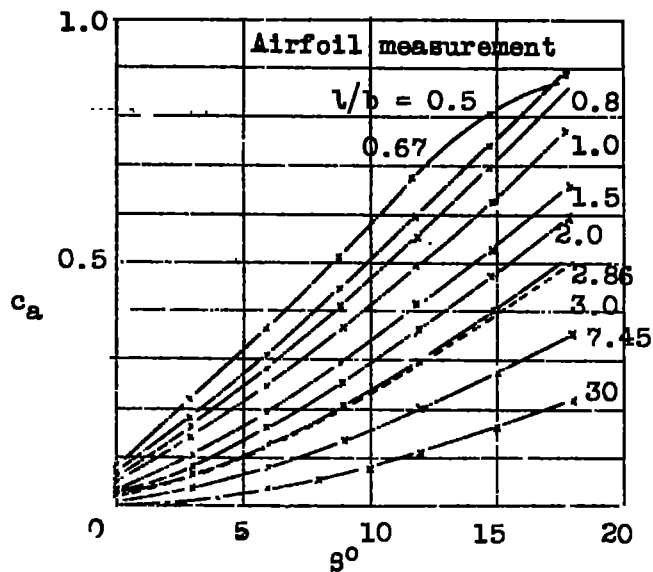Figures 23,24,25.- Photographs of surface pushed by water.

Figure 26.- Winter's airfoil with bevelled leading and
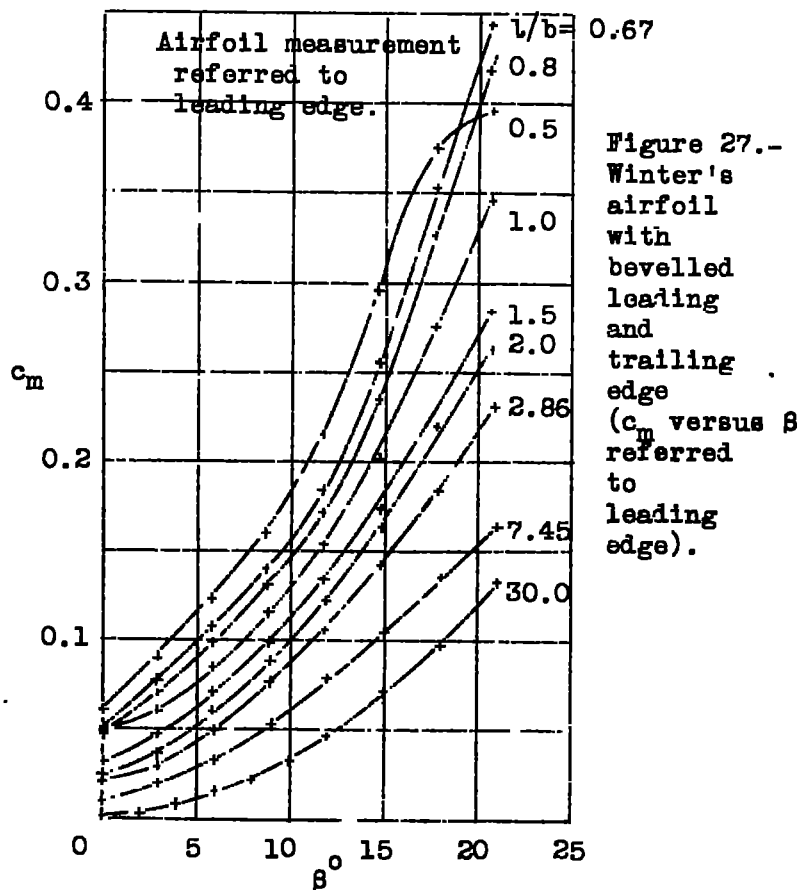trailing edge(c_a against β).

Figure 27.-
Winter's
airfoil
with
bevelled
leading
and
trailing
edge
(c_m versus β
referred
to
leading
edge).
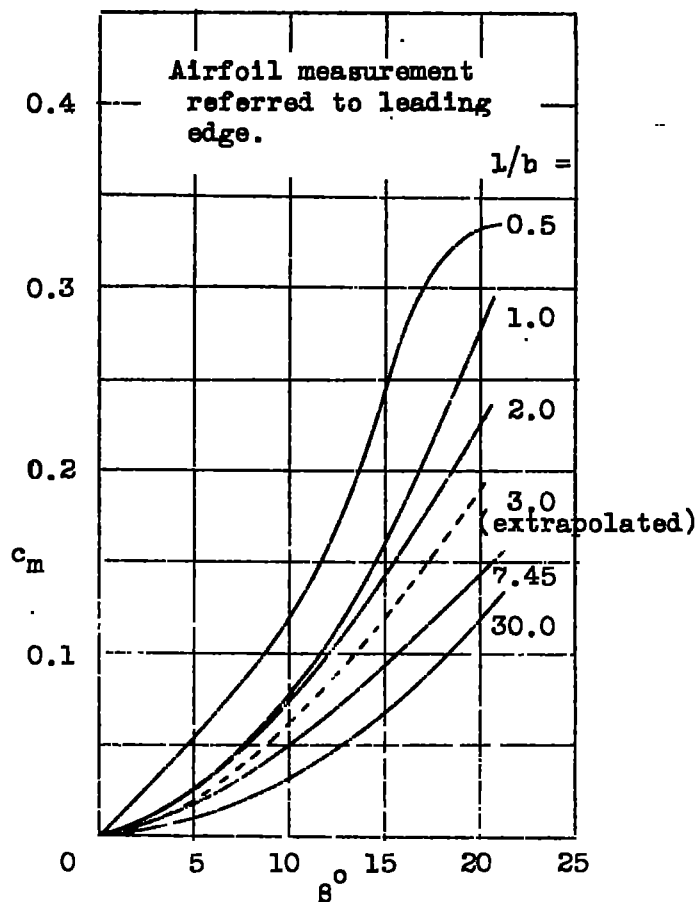
Figure 28.- Winter's airfoil data following elimination
             of leading and trailing edge bevel(c_m against β
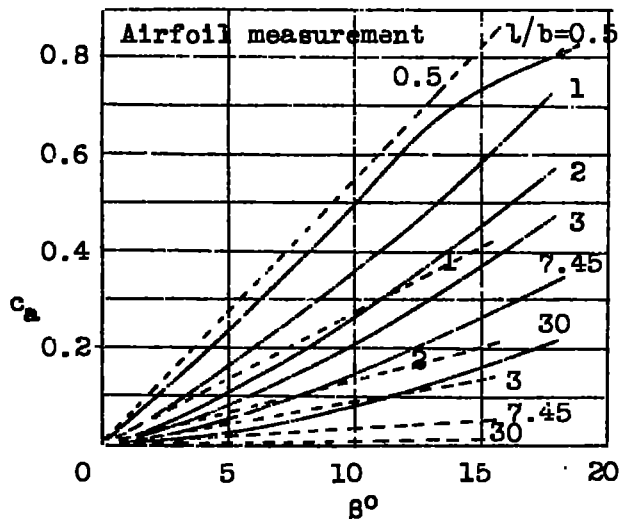referred to leading edge).

Figure 29.- Winter's airfoil data following elimination
             of leading and trailing edge bevel(c_a against β
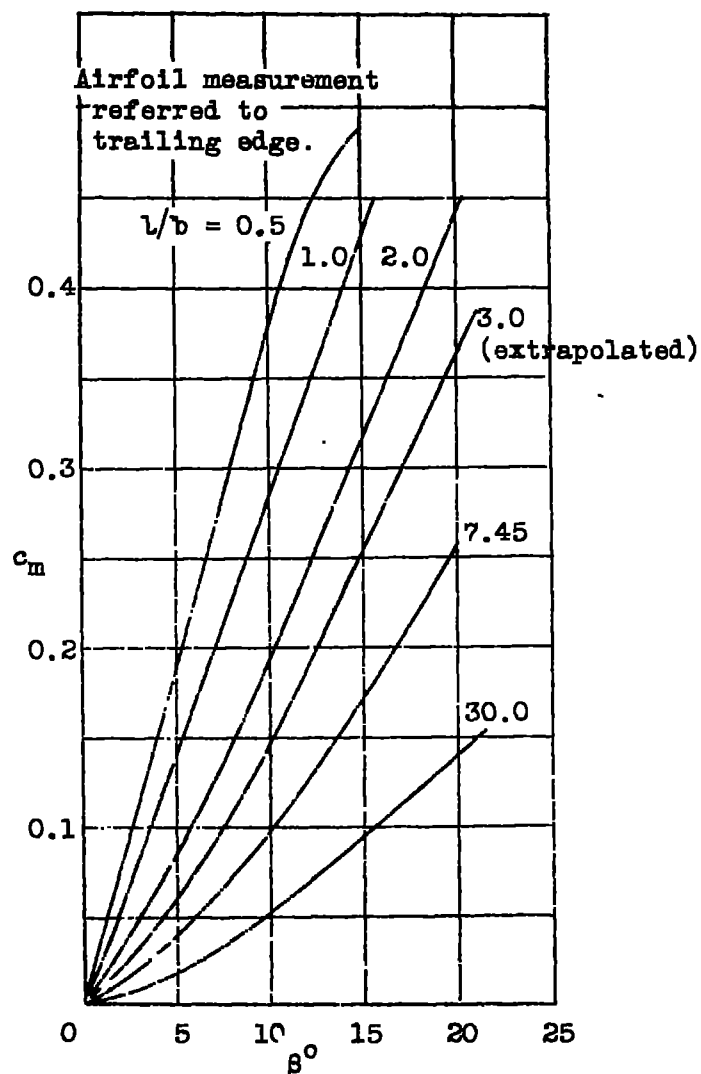referred to leading edge).

Figure 30.- Fig. 28 converted for airfoil trailing edge.

DO NOT REMOVE SLIP FROM MATERIAL

Delete your name from this slip when returning material to the library.

NAME	DATE	MS
D. Tomek	4/14/97	339

NASA Langley (Rev. Dec. 1991)   RIAD N-75